Structure of glycerol-3-phosphate dehydrogenase, an essential monotopic membrane enzyme involved in respiration and metabolism

Joanne I. Yeh[†‡§], Unmesh Chinte[†], and Shoucheng Du[†]

Departments of [†]Structural Biology and [‡]Bioengineering, University of Pittsburgh School of Medicine, 3501 5th Avenue, BST3 1036, Pittsburgh, PA 15260

Communicated by Angela M. Gronenborn, University of Pittsburgh, Pittsburgh, PA, January 2, 2008 (received for review November 15, 2007)

Sn-glycerol-3-phosphate dehydrogenase (GlpD) is an essential membrane enzyme, functioning at the central junction of respiration, glycolysis, and phospholipid biosynthesis. Its critical role is indicated by the multitiered regulatory mechanisms that stringently controls its expression and function. Once expressed, GlpD activity is regulated through lipid-enzyme interactions in *Escherichia coli*. Here, we report seven previously undescribed structures of the fully active *E. coli* GlpD, up to 1.75 Å resolution. In addition to elucidating the structure of the native enzyme, we have determined the structures of GlpD complexed with substrate analogues phosphoenolpyruvate, glyceric acid 2-phosphate, glyceraldehyde-3-phosphate, and product, dihydroxyacetone phosphate. These structural results reveal conformational states of the enzyme, delineating the residues involved in substrate binding and catalysis at the glycerol-3-phosphate site. Two probable mechanisms for catalyzing the dehydrogenation of glycerol-3-phosphate are envisioned, based on the conformational states of the complexes. To further correlate catalytic dehydrogenation to respiration, we have additionally determined the structures of GlpD bound with ubiquinone analogues menadione and 2-*n*-heptyl-4-hydroxyquinoline *N*-oxide, identifying a hydrophobic plateau that is likely the ubiquinone-binding site. These structures illuminate probable mechanisms of catalysis and suggest how GlpD shuttles electrons into the respiratory pathway. Glycerol metabolism has been implicated in insulin signaling and perturbations in glycerol uptake and catabolism are linked to obesity in humans. Homologs of GlpD are found in practically all organisms, from prokaryotes to humans, with >45% consensus protein sequences, signifying that these structural results on the prokaryotic enzyme may be readily applied to the eukaryotic GlpD enzymes.

electron transfer | glycerol metabolism | glyceroneogenesis | ubiquinone

Glycerol, glycerol-3-phosphate (G3P), and glycerophosphodiesters are carbon sources and precursors for phospholipid biosynthesis. Dissimilation of these central metabolic intermediates is carried out by the enzymes encoded by the *glp* regulon (1–3). Many organisms can use glycerol in metabolic processes that convert glycerol to precursors used for synthesis of essential cellular components, including lipids and cell wall. Consequently, the ability to metabolize glycerol is important for meeting the energy needs of many organisms and in processes related to signaling, catabolism, and respiration in eukaryotes.

The inner membrane of *Escherichia coli* is involved in a wide variety of functions essential to cell survival. The membrane-associated glycerol-3-phosphate dehydrogenase (GlpD) is one of the key flavin-linked primary dehydrogenases of the respiratory electron transport chain and serves an essential function for aerobic growth on glycerol (1–3). GlpD catalyzes the oxidation of G3P to dihydroxyacetone phosphate (DHAP), with concurrent reduction of flavin adenine dinucleotide (FAD) to $FADH_2$, and passes electrons on to ubiquinone (UQ) and ultimately to oxygen or nitrate (Fig. 1). GlpD is localized to the cytoplasmic membrane in *E. coli* and may constitute as much as 10% of the inner membrane proteins in constitutive strains, exhibiting membrane-dependency for activity (4–6). In eukaryotes, GlpD is located on the inner mitochondrial membrane and like succinate dehydrogenase (7), acyl CoA dehydrogenase (8), and complex II (succinate ubiquinone oxidoreductase) (9), GlpD channels electrons into the respiratory chain by reducing UQ. GlpD plays a critical role in shuttling reducing equivalents from cytosolic NADH into the mitochondrial matrix. These electron-transferring enzymes all contribute to the pool of reduced ubiquinone (UQH_2). UQH_2 from all these reactions is reoxidized by complex III, the next component in the mitochondrial electron-transfer chain.

The importance of the G3P shuttle is highlighted by the relative abundance of GlpD, which can exist in one of two isoforms: a soluble GlpD [also referred to as the oxidase, α-GlpO (10)] and a membrane-bound form, GlpD. The sequence identity can be >40%, as with the *Enterococcus casseliflavus* α-GlpO to the membrane-incorporated GlpD from *Bacillus subtilis*; however, only low levels of identity (≈17–20%) result from comparisons with other FAD-dependent oxidases (10). Further signifying its importance, the expression of GlpD is highly regulated and homologs of GlpD are found in practically all organisms. The complex interplay between various proteins in glycerol metabolism serves to regulate energy processes, having consequences on respiration and oxidative metabolism (11). Stringent two-tiered regulation of this pathway is by means of both transcriptional activation and membrane localization, which ensures GlpD is fully active only when it is associated with the cytoplasmic membrane or when reconstituted with phospholipids or amphiphiles *in vitro*. These mechanisms ensure that cellular energy needs are met while lipid biosynthesis is not disrupted (1–5, 11). To structurally characterize this important enzyme, we have determined the structures of GlpD in its native form and cocrystallized with substrate analogues, product, and UQ analogues (Tables 1 and 2).

Results

Topology, Domains, and Enzyme-Detergent Interactions. The structure of GlpD represents a previously structurally uncharacterized class of membrane-bound G3P dehydrogenases. The structure was determined through a three-wavelength seleno anomalous phasing approach (Table 1). *De novo* phasing was required, particularly as one domain embodies an unusual fold, not previously exhibited according to DALI (12) and CATH (13) searches, further elabo-

Author contributions: J.I.Y. designed research; J.I.Y., U.C., and S.D. performed research; J.I.Y. contributed new reagents/analytic tools; J.I.Y., U.C., and S.D. analyzed data; and J.I.Y. wrote the paper.

The authors declare no conflict of interest.

Freely available online through the PNAS open access option.

Data deposition: The atomic coordinates and structure factors have been deposited in the Protein Data Bank, www.pdb.org [PDB ID codes 2QCU (native GlpD), 2R4J (SeMet-GlpD), 2R45 (GlpD-2-PGA), 2R46 (GlpD-PEP), and 2R4E (GlpD-DHAP)].

[§]To whom correspondence should be addressed. E-mail: jiyeh@pitt.edu.

This article contains supporting information online at www.pnas.org/cgi/content/full/0712331105/DC1.

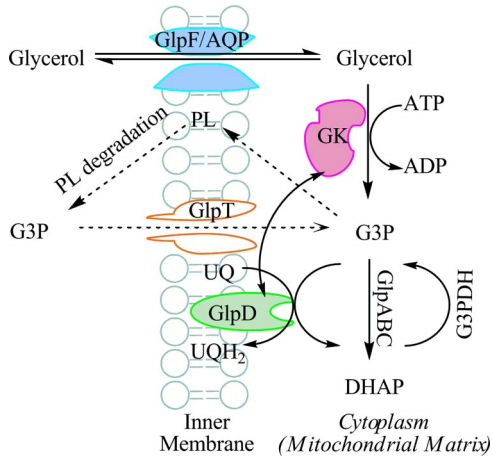

Fig. 1. Schematic of the glycerol metabolic pathway in *E. coli*. Protein members of the glycerol metabolic pathway includes glycerol facilitator (GlpF/AQP), a member of the aquaporin family of major intrinsic proteins. The soluble glycerol kinase (GK) phosphorylates glycerol to G3P. Another membrane protein constituent of this pathway is the transporter for the uptake of G3P (GlpT) with concomitant exit of Pi. Oxidation of G3P to DHAP is catalyzed by the monotopic membrane enzyme, glycerol-3-phosphate dehydrogenase (GlpD), a primary dehydrogenase. Concurrent with oxidation of G3P is reduction of flavin adenine dinucleotide (FAD) to $FADH_2$, which passes on electrons to ubiquinone (UQ) forming the reduced form (UQH_2) and ultimately shuttling electrons to oxygen or nitrate.

rated under Discussion. We have determined the structures of the native enzyme and in complex with product (DHAP, 2.1 Å) and in separate complexes with substrate analogues, glyceraldehyde-3-phosphate (GAP, 2.9 Å), glyceric acid 2-phosphate (2-PGA, 2.3 Å), and phosphoenolpyruvate (PEP, 2.1 Å). These are all competitive inhibitors to *E. coli* and mitochondrial GlpDs (4, 14, 15). We have additionally determined the structures of GlpD in complex with UQ analogues, menadione (MD, 2.6 Å) and 2-n-heptyl-4-hydroxyquinoline *N*-oxide (HQNO, 2.9 Å) to more fully correlate dehydrogenation to electron transfer; all data statistics are listed in Table 2.

GlpD comprises two major domains, a soluble extramembraneous C-terminal "cap" domain encompassing residues 389–501 and a N-terminal FAD-binding region that is part of the membrane-embedded domain, the "FAD-domain," consisting of the substrate-binding and base regions, comprised of residues 1–388 (Fig. 2). The distance from the surface of the "entrance/exit cleft" ("EEC," Fig. 2) to the isoalloxazine ring of FAD is ≈18 Å, with a diameter of 12 Å at the widest point at the entrance and narrows to ≈8 Å as the cleft is further penetrated. The dimeric enzyme is formed by monomers related by a noncrystallographic 2-fold axis of symmetry and the dimer comprises the unique asymmetric unit.

Electrostatic surface calculations show distinct regions of highly positive patches (in blue, Fig. 3), located at the base region of the enzyme. These regions are likely involved with the negatively charged membrane phospholipid head groups. The cap domain, at the opposite side, exhibits highly negatively electrostatic potential (in red, Fig. 3), with large hydrophobic patches between these two distal regions of the enzyme, forming membrane interaction and proposed UQ-binding surfaces.

At 1.75 Å resolution for the native enzyme, our data reveals five β-OG molecules interacting directly with a GlpD dimer, with four molecules of β-OG detergent molecules found at the base of the enzyme. The locations of these detergents are conserved in all of the structures and delineate the depth into which GlpD penetrates the bilayer (Fig. 2).

Mapping of Detergent Interaction Regions by Means of Limited Proteolysis. The necessity for lipids or detergents for solubilization and activity of *E. coli* and mitochondrial GlpD are well documented; activity of GlpD can be reconstituted *in vitro* by means of detergent substitution (4–6, 14, 15). Removal of detergent results in a dramatic reduction in activity, which can be restored by addition of phospholipids (4, 5); these results have been verified [supporting information (SI) Table 3]. Structurally, detergent requirement for *in vitro* GlpD activity can be explicated not only by the need to protect lipid-protein interaction surfaces but additionally by the distribution of apolar/hydrophobic residues highlighting the significant role of detergent/lipids for maintaining the conformational integrity of the enzyme (Fig. 3).

To further map solvent-exposed and membrane-embedded regions, we conducted limited proteolysis-membrane/detergent protection experiments coupled with mass spectrometry (MS) to map phospholipid- and detergent-interaction surfaces of GlpD. We reconstituted the enzyme separately in β-OG and *E. coli* phospholipids. Another member of the glycerol metabolism pathway, glycerol kinase (16) (GK), was used as a control as GK has comparable topology–a dimer with similar buried surface areas (≈1,500 Å^2 in GK, ≈1,600 Å^2 in GlpD) and trypsin cut sites (52 in GK, 59 in GlpD) but is a soluble enzyme. After 30 min of digestion, MS analysis showed that >86% of GK (in β-OG) was proteolyzed whereas in GlpD only 40% (in β-OG) and 43% (in *E. coli* lipids) were proteolyzed, as tabulated in SI Table 4. Replicates of three digestion experiments clearly segregate the regions protected by detergent or lipid interactions; these regions are clustered at the MD/HQNO-binding plateau, the base region that interacts with the membrane and additionally at the dimer interface (SI Fig. 5).

Active Site and Probable Ubiquinone Docking Site. In addition to the four β-OG molecules found at the base of the FAD-binding domain, an additional detergent molecule was found bound to a hydrophobic plateau with well resolved electron density; representative densities of the β-OG detergent molecule and the FAD at the active site are shown in SI Fig. 6. To address whether this region

Table 1. Data collection, phasing and refinement statistics for MAD (SeMet) structure

	GlpD-SeMet		
Data collection			
Space group		1222	
Cell dimensions			
a, *b*, *c*, Å		113.92, 114.14, 193.59	
α, β, γ, °		90, 90, 90	
	Peak	Inflection	Remote
Wavelength	0.97928	0.97947	0.97181
Resolution, Å	1.95	2	2.15
R_{sym} or R_{merge}	0.113	0.126	0.082
$I/\sigma I$	13.1	11.6	19.3
Completeness, %	96.5	98.4	98.2
Redundancy	6.3	6.1	7.1
Refinement			
Resolution, Å		1.95	
No. of reflections		90,203	
R_{work}/R_{free}		0.215/0.243	
No. of atoms			
Protein		8,014	
Ligand/ion		126	
Water		174	
B-factors			
Protein		35.059	
Ligand/ion		30.195	
Water		40.802	
rmsd			
Bond lengths, Å		0.017	
Bond angles, °		1.9	

BIOCHEMISTRY

Table 2. Data collection and refinement statistics

	Native	2-PGA	PEP	DHAP	GAP	MD	HQNO
Data collection							
Space group	I222	I222	I222	I222	I222	I222	I222
Cell dimensions							
a, *b*, *c*, Å	113.95, 114.19, 193.16	113.75, 113.91, 193.07	114.02, 114.09, 193.16	113.71, 113.74, 193.03	116.02, 116.13, 195.56	115.71, 115.93, 195.60	114.10, 114.49, 192.62
α , β , γ , °	90, 90, 90	90, 90, 90	90, 90, 90	90, 90 ,90	90, 90, 90	90, 90, 90	90, 90, 90
Resolution, Å	1.75	2.3	2.1	2.1	2.9	2.6	2.9
R_{sym} or R_{merge}	0.06 (0.442)	0.089 (0.435)	0.079 (0.401)	0.076 (0.384)	0.087 (0.425)	0.081 (0.386)	0.102 (0.507)
$I/\sigma I$	12.9 (3.0)	14.5 (1.8)	9.2 (3.1)	21.1 (2.6)	11.0 (3.2)	8.9 (2.3)	7.0 (2.9)
Completeness, %	99.6 (99.1)	98.5 (88.1)	100 (100)	99.9 (99.1)	91.4 (82.4)	93.2 (85.8)	99.9 (100)
Redundancy	9.4 (9.3)	6.2 (3.6)	9.9 (10.0)	6.1 (5.0)	7.3 (5.9)	4. 5 (3.6)	7.4 (7.5)
Refinement							
Resolution, Å	1.75	2.3	2.1	2.1	2.9	2.6	2.9
No. of reflections	125,835	55,867	73,532	73,805	27,093	37,943	2,8342
R_{work}/R_{free}	0.19/0.235	0.189/0.238	0.197/0.25	0.191/0.25	0.185/0.283	0.216/0.262	0.182/0.282
No. of atoms							
Protein	8,014	8,014	8,014	8,014	8,014	8,014	8,014
Ligand/ion	106	128	126	126	126	165	164
Water	472	378	300	400			
B-factors							
Protein	29.1	37.6	35.1	34.1	35.2	37.4	38.0
Ligand/ion	17.3	26.0	23.6	24.6	27.0	39.6	39. 7
Water	35.8	36.8	39.0	39.5			
rmsd							
Bond lengths, Å	0.013	0.019	0.022	0.023	0.025	0.025	0.025
Bond angles, °	1.7	1.9	2.2	2.2	2.5	2.5	2.5

Values in parentheses are for highest-resolution shell.

could be the UQ docking site, we determined the structures of GlpD bound with menadione (MD) and 2-*n*-heptyl-4-hydroxyquinoline *N*-oxide (HQNO), to resolutions of 2.6 and 2.9 Å, respectively (Table 2). MD is a bacterial UQ analog, used in enzymatic reactions with GlpD to establish its electron-transfer activity (4) whereas HQNO is competitive inhibitor that can bind to UQ-sites (17); we have determined the activity of GlpD in the presence of MD and HQNO, further verifying that these quinones can function to accept electrons generated from dehydrogenation of G3P or have inhibitory effects on electron transfer to the terminal acceptor in the assay (SI Table 5). The MD and HQNO sites are close to the hydrophobic plateau region initially indicated by the β-OG molecule; difference Fouriers maps for three separate datasets of MD- and HQNO-complexed GlpD were compared and all define binding to the hydrophobic plateau, with well resolved electron densities except for the flexible tail region of HQNO (SI Fig. 7). MD and HQNO can displace β-OG in the soaked structures, indicating greater binding affinities. Although it has been speculated that GlpD is a metalloenzyme (4), in contrast, we found GlpD to be inhibited by metals, similar to the human dehydrogenase, Gpd1 (18). The metal-independency for GlpD activity may have implications on the mechanism of electron transfer, discussed below.

Structural evidence that this region is the UQ docking site is that a number of β-strands are found here, presenting a planar lipophilic surface, similar to that observed in electron-transfer flavoprotein-ubiquinone oxidoreductase (ETF-QO) (19). Additionally, the presence of a topological switch point, whereby two adjacent parallel β-strands form a substrate binding cleft with their respective loops,

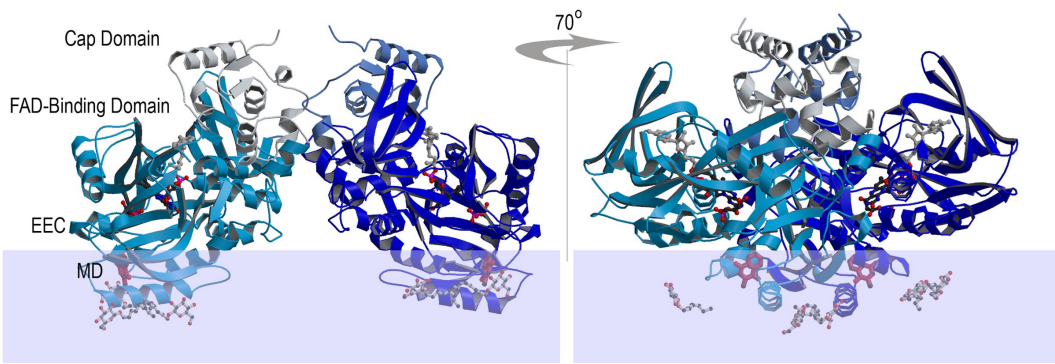

Fig. 2. Dimeric structure of the glycerol-3-phosphate dehydrogenase. Two views of the GlpD enzyme, in ribbon depiction, with the membrane bilayer indicated by the transparent blue rectangle. A molecule of FAD and product DHAP, depicted in ball-in-stick at the center of each monomer, defines the active site in the dimeric GlpD. β-octyl glucoside detergent (β-OG) molecules, depicted in ball-and-stick, are found at the base of the enzyme. A UQ analogue, menadione (MD), is found bound at a hydrophobic plateau, possibly delineating the UQ docking site.

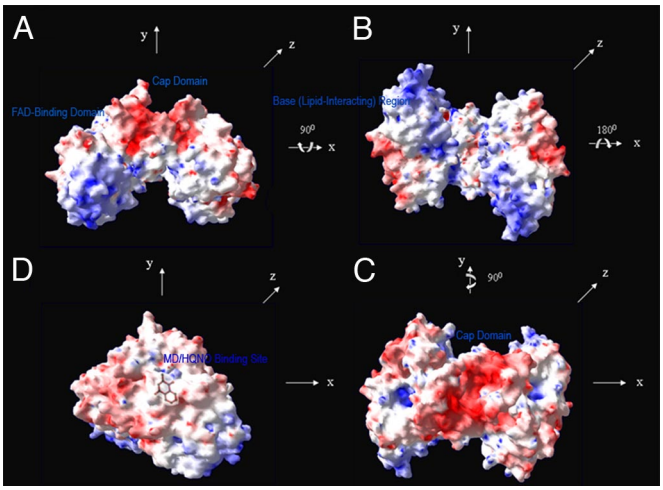

Fig. 3. Electrostatic potential maps. Electrostatic potential surfaces in blue for positive (+8kT), white for hydrophobic, and red for negative (−kT). High positive potentials at found at the base region, defining surfaces likely to be involved in interacting with the negatively charged phospholipid head groups of the membrane. (*A*) With the cap domain at top, distinct segregation of potentials with clustering of negative potentials at one end (cap) and positive potentials at the opposite end (base of the FAD-domain). (*B*) Shown 90° from *A*, looking up at the base, regions of extensive hydrophobic patches are found, in white. (*C*) Shown 180° from *B*, view looking down the red cap domain, with the hydrophobic surfaces located at periphery of GlpD. (*D*) Shown 90° from *C*, a hydrophobic plateau is found with a MD bound and may be the putative UQ docking site.

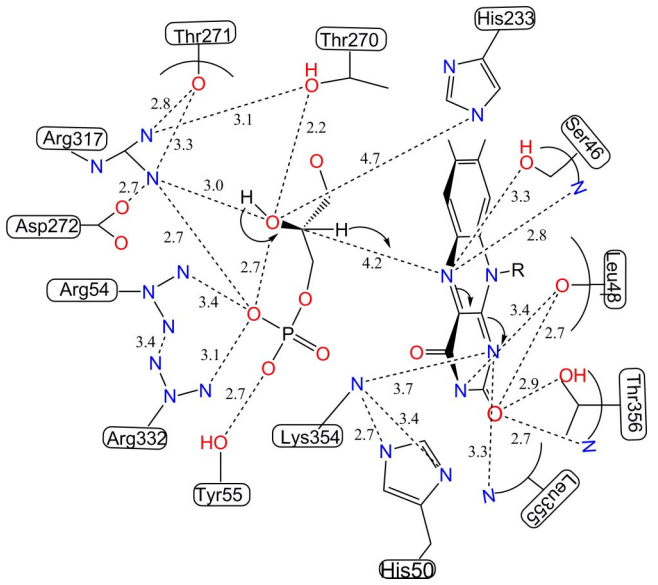

Fig. 4. Reaction scheme. Schematic diagram showing the active site with G3P, modeled from the GAP-complex structure. Only selected interactions in the active site are shown. Dotted lines indicate distances, in angstroms, between atoms in proximity for hydrogen bonding interactions. For FAD, only the isoalloxazine ring is depicted.

further signify a physiological binding site (20). In the GlpD, this switch point is somewhat unusual in that the loops do not form the "classical" binding cleft whereby the loops diverge but rather point in a similar direction. This anomaly may be due to the presence of aromatics and overall abundance of hydrophobic residues found at this region.

Discussion

We present the structure of a monotopic membrane enzyme class of G3P dehydrogenases, in multiple complexed states. A DALI search (12) of the NT-FAD domain shows good alignments of the substrate-binding regions with other oxidases and dehydrogenase, with a *Z* score of 34.5, 2.5 Å rmsd, and 15% sequence identity between the closest identified protein, glycine oxidase. This similarity is expected for the FAD-binding region as this motif is conserved structurally across many flavoproteins. However, for the CT-cap domain, the highest *Z* score is 5.3 with 3 Å rmsd and 5% sequence identity to a hypothetical protein from *Pyrococcus horikoshii*, ph1363. A CATH analysis (13), which attempts to find the closest fold group for a given protein structure, was also conducted. The most similar structure identified through CATH (PDB ID: 1NJG, chain B) resulted in a rmsd value of 7 Å. The SSAP and CATH scores were 61.3 and 4.28, respectively. Consequently, these analyses indicate that the cap-domain embodies an unusual fold as structures with high sequence identity (>35%) and structural similarity results in SSAP scores >80 and with significantly lower rmsd values.

Another striking feature of the cap domain is the overall negative electrostatic surface (in red, Fig. 3*C*), which may aid in substrate recognition. The positive electrostatic potential of the base of the FAD-domain (in blue, Fig. 3 *A* and *B*) delineates the regions that interacts with the negative phospholipid head groups of the membrane bilayer. The distinct electrostatic "polarity" of these distal regions likely aid in ensuring proper alignment of GlpD into the membrane bilayer. These results, together with the conserved detergent molecules located at the base of this domain and additional large hydrophobic surfaces on GlpD helps to demarcate the membrane-interacting regions. Based on these considerations and the distribution of polar and hydrophobic residues located at the base of the FAD-binding domain and the location of the proposed UQ hydrophobic plateau, we estimate that GlpD embeds to depths of ≈12–15 Å into the lipid bilayer (Fig. 2). We have confirmed previous reports that *E. coli* GlpD activity is not only dependent on membrane or detergent interactions but also exhibits preference to certain amphiphiles (5) (SI Table 3) and can be functionally reconstituted with *E. coli* membrane vesicles to support G3P-dependent active transport of L-proline (4). GlpD from *B. subtilis* and several mitochondrial GlpDs have been characterized and all require exogenous phospholipids or nondenaturing detergents for electron-transfer activity (4–6, 14, 15).

The GlpD enzyme exhibits a relatively high hydrophobic content distributed throughout the protein; dimer formation seems to be requisite, to protect these extensive hydrophobic surfaces. Criterion for identifying true oligomeric protein–protein contacts uses a buried solvent accessible surface area of 400 Å^2 as a lower-limit and up to ≈850 Å^2 to discriminate between monomeric and homodimeric proteins (21, 22). In GlpD, the monomer interface form extensive interactions with a contact (buried) surface area of 1,626.4 Å (2), strongly signifying that the dimeric structural state determined crystallographically is the physiologically relevant dimer.

Dehydrogenation occurs at a protected active site formed via the dimer interface and through the folded protein scaffold; the PEP, 2-PGA, GAP, and DHAP complexes define the active site interactions (SI Fig. 8). The catalytic center is shielded from solvent, providing an apolar microenvironment required for catalysis that has been observed in other flavoenzymes (23, 24). In GlpD, the isoalloxazine ring forms numerous interactions with the protein polypeptide on the *si*-side; residues in proximity of 3.4 Å or less are Ser-46, Leu-48, His-50, Leu-355, and Thr-356. These residues form intimate interactions with the FAD so substrates can only bind at the *re*-face of the isoalloxazine ring. The binding interactions with the phosphate group of the substrates are conserved in all of the structures, possibly serving as the initial anchor-point that aligns the substrate for dehydrogenation (Fig. 4).

Binding of the substrate-analogs and DHAP are mediated through residues Arg-54, Tyr-55, Thr-270, Thr-271, Arg-272, Arg-317, and Arg-332. At the active site, Arg-317 is in proximity to the hydroxyl group of C2 of GAP; consequently, we propose that Arg-317 acts as a general base to catalyze the abstraction of a proton in G3P. In this scheme, Arg-317 first deprotonates the hydroxyl group (O2) of C2 in G3P to initiate the dehydrogenation reaction (Fig. 4). Hydride transfer from C2 of G3P to N5 of FAD results in the dihydroflavin anion state. The C2 position of GAP is in proximity to N5 of the flavin at 4.2 Å; this distance suggests complexation with the endogenous substrate, G3P, likely induces a conformational shift of ≈1 Å so that the transition state distances would be more optimal for direct hydride transfer. The proposed direct hydride transfer mechanism is consistent with those elaborated for D-amino acid oxidase (25), PutA669 (26), and complex II (27). The reduced flavin is stabilized by Lys-354 (Fig. 4), which is positioned under the isoalloxazine ring at 3.7 Å from N1 with additional stabilization by the backbone nitrogen of Leu-355. A protein positive charge near the flavin N1 locus is a distinguishing feature of most flavoprotein oxidases, with mechanistic implications for the modulation of flavin reactivity (24). Comparative analysis with other flavoenzyme structures clusters the site of oxidative attack with substrates ≈3.5 Å distance from N5, defining an angle with the N5-N10 atoms in the narrow range of 96–177° (23).

Our proposal of Arg as the catalytic base is similar to the reaction suggested for complex II (27), where Arg-297 acts as a general base catalyst. Distances from Arg-297 in complex II to the C3 and O4 of the oxaloacetate (a substrate analogue) are 3 Å. Arg as the active site base is also proposed in fumarate reductase (28) and IMP dehydrogenase (29). Additionally, in complex II, hydrogen bonding between the guanidinio nitrogens of Arg-297 to carboxylates were proposed to increase the basicity of this residue (27). Analogously, in GlpD, a guanidino nitrogen of Arg-317 H-bonds to a phosphate oxygen and to Asp-272 (Fig. 4), likely perturbing the pK_a of Arg-317.

His-233 remains a viable candidate as the catalytic base in GlpD although the distance between His-233 NE2 to the O2 atom of GAP is 4.7 Å and thus not as optimal as Arg-317; however, there are numerous examples of His-mediated dehydrogenation. To illustrate, His-447 abstracts the C3-hydroxyl proton of cholesterol in cholesterol oxidase (30). It is possible that His-233 in GlpD can perform this function on the hydroxyl proton of C2 in G3P although at 4.7 Å, this mechanism is less probable. There may be unexpected conformational changes once the endogenous substrate, G3P, binds although based on the complex structures presented here, Arg-317 seems to be more likely as the conformation of His-233 remains invariant in all structures.

The *in vivo* acceptor of reducing equivalents generated from dehydrogenation of G3P in GlpD has been proposed to be Q8 (5, 11). The MD/HQNO location we identified is plausible as this docking site would place UQ in proximity to the active site, to accept electrons generated concomitantly with oxidation of G3P to DHAP. The closest atomic distance between MD to FAD is 11.6 Å (C7 of MD to C7 of FAD); when measured from C7 of MD to N5 of FAD, the distance is 15 Å (SI Fig. 9). No other cofactors or metals seem to be required for GlpD activity nor metal clusters, such as FeS-clusters in the case of ETF-QO (19). Lack of additional cofactors suggests that electron transfer from $FADH_2$ to UQ may be mediated through protein residues or that a ping-pong type mechanism may function whereby the product, DHAP, first exits the cleft, permitting UQ access to $FADH_2$ for reduction. In the second mechanism, the presence of DHAP in the MD- and HQNO-soaked crystals may have prevented MD/HQNO from further penetrating the active site. The topological similarity of the UQ-binding plateau in GlpD and ETF-QO may also reflect a certain amount of conservation in the electron transfer mechanism used in the membrane-bound GlpD and other flavin-linked dehydrogenases including complexes I, II (9, 31), cytochrome bc1 (complex III) (32), and dihydroorotate dehydrogenase (33), as these enzymes all funnel electrons into the respiratory chain.

Limited proteolysis has been used extensively, most notably with bacteriorhodopsin (34) and GlyR (35); the validity of this approach to map membrane–protein interaction regions was verified once the crystal structure of bacteriorhodopsin was determined, confirming that proteolytic cleavages were not detected within the protected membrane-interacting regions of the protein (36). Our results from limited proteolysis-MS analysis cluster the protected regions, defining protein-membrane interaction surfaces and correlates well with our structural results. The similarity in the protection pattern in β-OG micelles and *E. coli* lipid-reconstituted GlpD and preservation of activity when reconstituted in β-OG and membrane extracts, provide evidence that our three-dimensional structures are physiologically sound.

The structure of the membrane-dependent GlpD enzyme reported here is one of only a handful of monotopic membrane proteins that have been structurally characterized; to our knowledge, the GlpD structure is one of the highest resolution structure determined to date of this class of membrane proteins. Monotopic membrane proteins are submerged from one side of the membrane into the nonpolar part of the lipid bilayer, without protruding through it. In these structures, the molecular 2-fold axis relating the monomers within the dimer is perpendicular to the membrane. This topology seems to be conserved in monotopic membrane proteins and may aid in orienting the nonpolar regions so they are parallel to the surface of the membrane, augmenting their tendencies to enter the lipid.

Our structural and biochemical results provide insights into the function and regulation of enzymes involved in the complex interplay between sugar and glycerol metabolism pathways. Recent reports highlight the central role of glycerol in intermediary metabolism and alterations in glycerol processing and transport can have significant pleiotropic effects on lipid accumulation, insulin sensitivity, and glucose homeostasis (37, 38). New findings indicate that glyceroneogenesis may have profound effects on repatterning energy metabolism and may lead to greater longevity in mice (39). The structures presented here provide a basis for addressing further questions about electron-transfer and catalytic mechanisms mediated by this important class of membrane-dependent enzymes, which link the essential cellular pathways of respiration, glycolysis, and lipid biosynthesis.

Methods

Expression, Purification, and Detergent Reconstitution of GlpD. GlpD was expressed, detergent extracted, purified, and assayed as published (40). As detailed in the earlier report, detergent screening to maintain the activity of GlpD was conducted; for the structural and biochemical studies reported here, 1-O-*n*-octyl-β-D-glucopyranoside (β-OG; MW 292.4) was used as the detergent.

Selenomethionine-labeled GlpD (GlpD-SeMet) was expressed by using a modified methionine pathway inhibition method; complete selenomethionine substitution in GlpD was confirmed by mass spectrometry analysis. Additional experimental details for all methods are supplied in *SI Methods*.

Native GlpD and GlpD-SeMet Crystallization. Purified GlpD and GlpD-SeMet in 20 mM Tris·HCl, pH 7.5, 0.5 M NaCl, 0.5 M imidazole and 1% OG, were concentrated to 8 mg/ml and crystallized at 4°C from a solution containing 0.1 M di-ammonium hydrogen phosphate, 0.1 M bicine pH 8.5, and 12% wt/vol PEG 6000. Three-wavelength anomalous data were collected at SER-CAT beamline ID-22 (Advanced Photon Source, Argonne National Laboratory; Table 1).

GlpD Cocrystallization with Substrate Analogues. GlpD cocrystallized with product DHAP and separately with substrate analogues were obtained by adding PEP and 2-PGA to the protein stock to a final concentration of 5 mM. Single wavelength datasets for native and complex crystals of GlpD bound with DHAP, PEP, and 2-PGA were collected at the Swiss Light Source, beamline X10A (Villigen, Switzerland; Table 2).

GlpD Soaked with Ubiquinone Analogues and Substrate Analogue, GAP. Soaking experiments were carried out by transferring GlpD-DHAP crystals from the original drop to a sitting drop containing 4 μl of the crystallization solution supplemented with 4% more of PEG 6000 and either MD or HQNO at 2.5 mM, then incubated at 4°C. Crystals were screened starting after 24 h of soaking and the best data were collected from crystals soaked for 42 h (MD) and 78 h (HQNO). GlpD crystals were soaked as described above except substituting GAP to a final concentration of 5 mM. Screening of GAP crystals were done as described above (Table 2). To cryocool, the soaked crystals were transferred to a cryo solution supplemented with 30% ethylene glycol (final concentration); crystals were looped out and flash-cooled in liquid nitrogen.

Structure Determination. The selenomethionine GlpD crystallized in space group I222 with a solvent content of ≈55% with two molecules in the asymmetric unit. Three-wavelength MAD datasets were collected at SER-CAT beamline ID-22. A total of 180 images with 1° frame width were collected at all three wavelengths with a crystal-to-detector distance of 250 mm. Exposure times were varied between 3 and 5 s. The crystal was translated after each wavelength during data collection due to radiation sensitivity. All datasets were processed by using HKL2000 suite (41) and D*TREK (42). Data collection and processing statistics are reported in Table 1.

Heavy atom positions were determined with a three-wavelength MAD dataset in SOLVE (43). Heavy atom positions and phases obtained from SOLVE were used for statistical density modification in RESOLVE in combination with refinement using refmac5 (44) and CNS (45). Noncrystallographic symmetry (NCS) averaging was performed in RESOLVE using the NCS matrix derived from heavy atom positions. The model obtained from RESOLVE had a working R of 37.5% and free R of 41.1%. Unbiased $F_{obs}e^{i\varphi calc}$ map obtained using the MAD phases showed continuous density for most of the backbone. Restrained refinements in refmac5 with simulated annealing refinement in CNS were iteratively checked by model fitting in $F_{obs} - F_{calc}$ and $F_{obs} - F_{calc}$ maps. Model building and fitting were done in Coot and solvent and substrate molecules were added by using ARP/wARP programs (46). Current refinement statistics for the native and in complex with DHAP, PEP, 2-PGA, GAP, MD, and HQNO are listed in Table 2. Further details of refinement and validation are supplied in *SI Methods*.

Mapping of β-OG and Lipid-Interacting Surfaces by Means of Limited Proteolysis-Mass Spectrometry Analysis. A time-dependent proteolysis profile was determined for the trypsin-protection experiments to map detergent and lipid-binding surfaces of GlpD. Tabulated results from three replicates for both the β-OG and phospholipid reconstituted samples are listed in SI Table 4; full experimental details are supplied in *SI Methods*.

Activity of GlpD in Presence of β-OG, Phosphlipids, Ubiquinones, and Substrate Analogues. Activity of GlpD was quantitated by determining the phenazine methosulfate (PMS)-coupled reduction of 2-(4,5-dimethyl-2-thiazolyl)-3,5-diphenyl-2*H*-tetrazolium bromide (MTT; ε = 17 $mM^{-1}{\cdot}cm^{-1}$); this reduction depends on glycerol-3-phosphate. The reaction is measured spectrophotometrically at 570 nm in the presence of 1% β-OG, as described (40). The ability of MD and HQNO to function as the electron-coupler in place of PMS was quantitated. The effects of various substrate analogues, phospholipids, and ubiquinones on activity were quantitated; these results are tabulated in SI Tables 3, 5, and 6.

ACKNOWLEDGMENTS. We thank Dr. Ehmke Pohl of the Paul Scherrer Institute, Swiss Light Source, for valuable technical expertise at the X10SA beamline. We thank Dr. Colin Thorpe, Dr. Vernon Anderson, and Dr. Edward Berry for insightful structural and mechanistic discussions. Data for SeMet-GlpD were collected at Southeast Regional Collaborative Access Team (SER-CAT) 22-ID beamline at the Advanced Photon Source, Argonne National Laboratory. This work was supported by National Institutes of Health Grant GM-66466 (to J.I.Y.). Use of the Advanced Photon Source is supported by the U.S. Department of Energy, Office of Science, Office of Basic Energy Sciences, under Contract W-31-109-Eng-38.

1. Austin D, Larson TJ (1991) Nucleotide sequence of the glpD gene encoding aerobic sn-glycerol 3-phosphate dehydrogenase of *Escherichia coli* K-12. *J Bacteriol* 173:101–107.
2. Beijer L, Nilsson R-P, Holmberg C, Rutberg L (1993) The glpP and glpF genes of the glycerol regulon in Bacillus subtilis. *J Gen Microbiol* 139:349–359.
3. Weissenborn DL, Wittekindt N, Larson TJ (1992) Structure and regulation of the glpFK operon encoding glycerol diffusion facilitator and glycerol kinase of *Escherichia coli* K-12. *J Biol Chem* 267:6122–6131.
4. Schryvers A, Lohmeier E, Weiner JE (1978) Chemical and functional properties of the native and reconstituted forms of the membrane-bound, aerobic glycerol-3-phosphate dehydrogenase of *Escherichia coli*. *J Biol Chem* 253:783–788.
5. Robinson JJ, Weiner JH (1980) The effect of amphipaths on the flavin-linked aerobic glycerol-3-phosphate dehydrogenase from *Escherichia coli*. *Can J Biochem* 48:1172–1178.
6. Weiner JH, Heppel LA (1972) Purification of the membrane-bound and pyridine nucleotide-independent L-glycerol 3-phosphate dehydrogenase from *Escherichia coli*. *Biochem Biophys Res Commun* 47:1360–1365.
7. Yankovskaya V, *et al*. (2003) Architecture of succinate dehydrogenase and reactive oxygen species generation. *Science* 299:700–704.
8. Battaile KP, *et al*. (2002) Crystal structure of rat short chain acyl-CoA dehydrogenase complexed with acetoacetyl-CoA: Comparison with other acyl-CoA dehydrogenases. *J Biol Chem* 277:12200–12207.
9. Sun F, *et al*. (2005) Crystal structure of mitochondrial respiratory membrane protein complex II. *Cell* 121:1043–1057.
10. Parsonage D, Luba J, Mallett TC, Claiborne, A (1998) The soluble α-glycerophosphate oxidase from *Enterococcus casseliflavus*. *J Biol Chem* 273:23812–23822.
11. Haddock BA, Jones CW (1977) Bacterial respiration. *Bacteriol Rev* 41:47–99.
12. Holm L, Sander C (1996) Mapping the protein universe. *Science* 273:595–603.
13. Pearl FM, *et al*. (2003) The CATH database: An extended protein family resource for structural and functional genomics. *Nucleic Acids Res* 31:452–455.
14. Garrib A, McMurray WC (1986) Purification and characterization of glycerol-3-phosphate dehydrogenase (flavin-linked) from rat liver mitochondria. *J Biol Chem* 261:8042–8048.
15. Cottingham IR, Ragan CI (1980) Purification and properties of L-3-glycerophosphate dehydrogenase from pig brain mitochondria. *Biochem J* 192:9–18.
16. Yeh JI, *et al*. (2004) Structures of enterococcal glycerol kinase in the absence and presence of glycerol: Correlation of conformation to substrate binding and a mechanism of activation by phosphorylation. *Biochemistry* 43:362–373.
17. Kogut M, Lightbown JW (1962) Selective inhibition by 2-heptyl-4-hydroxyquinoline *N*-oxide of certain oxidation-reduction reactions. *Biochem J* 84:368–382.
18. Ou X, *et al*. (2006) Crystal structures of human glycerol 3-phosphate dehydrogenase 1 (GPD1). *J Mol Biol* 357:858–869.
19. Zhang J, Frerman FE, Kim JJ (2006) Structure of electron transfer flavoprotein-ubiquinone oxidoreductase and electron transfer to the mitochondrial ubiquinone pool. *Proc Natl Acad Sci USA* 103:16212–16217.
20. Ye S, *et al*. (2001) The structure of a Michaelis serpin-protease complex. *Nat Struct Biol* 8:979–983.
21. Ponstingl H, Henrick K, Thorton JM (2000) Discriminating between homodimeric and monomeric proteins in the crystalline state. *Proteins Struct Funct Genet* 41:47–57.
22. Elcock AH, McCammon JA (2001) Identification of protein oligomerization states by analysis of interface conservation. *Proc Natl Acad Sci USA* 98:2990–2994.
23. Fraaije MW, Mattevi A (2000) Flavoenzymes: diverse catalysts with recurrent features. *Trends Biochem Sci* 25:126–132.
24. Ghanem M, Gadda G (2006) Effects of reversing the protein positive charge in the proximity of the flavin N (1) locus of choline oxidase. *Biochemistry* 45:3437–3447.
25. Pollegioni L, Blodig W, Ghisla S (1997) On the mechanism of D-amino acid oxidase. Structure/linear free energy correlations and deuterium kinetic isotope effects using substituted phenylglycines. *J Biol Chem* 272:4924–4934.
26. Lee L-H, Nadaraia S, Gu D, Becker DF, Tanner JJ (2003) Structure of the proline dehydrogenase domain of the multifunctional PutA flavoprotein. *Nat Struct Biol* 10:109–114.
27. Huang L-S, *et al*. (2006) 3-Nitropropionic acid is a suicide inhibitor of mitochondrial respiration that, upon oxidation by complex II, forms a covalent adduct with a catalytic base arginine in the active site of the enzyme. *J Biol Chem* 281:5965–5972.
28. Taylor P, Pealing SL, Reid GA, Chapman SK, Walkinshaw MD (1999) Structural and mechanistic mapping of a unique fumarate reductase. *Nat Struct Biol* 6:1108–1112.
29. Hedstrom L, Gan, L. (2006) IMP dehydrogenase: Structural schizophrenia and an unusual base. *Curr Opin Chem Biol* 10:520–525.
30. Yue QK, Kass IJ, Sampson NS, Vrielink A (1999) Crystal structure determination of cholesterol oxidase from *Streptomyces* and structural characterization of key active site mutants. *Biochemistry* 38:4277–4286.
31. Lenaz G (2001) A critical appraisal of the mitochondrial coenzyme Q pool. *FEBS Lett* 509:151–155.
32. Iwata S, *et al*. (1998) Complete structure of the 11-subunit bovine mitochondrial cytochrome bc1 complex. *Science* 281:64–71.
33. Rowland P, Nielsen FS, Jensen KF, Larsen S (1997) The crystal structure of the flavin containing enzyme dihydroorotate dehydrogenase A from *Lactococcus lactis*. *Structure (London)* 5:239–252.
34. Grigorieff N, Ceska TA, Downing KH, Baldwin JM, Henderson R (1996) Electron-crystallographic refinement of the structure of bacteriorhodopsin. *J Mol Biol* 259:393–421.
35. Leite JF, Amoscato AA, Cascio M (2000) Coupled proteolytic and mass spectrometry studies indicate a novel topology for the glycine receptor. *J Biol Chem* 275:13683–13689.
36. Leucke H, Schobert B, Richter HT, Cartailler JP, Lanyi JK (1999) Structure of bacteriorhodopsin at 1.55 A resolution. *J Mol Biol* 291:899–911.
37. Hara-Chikuma M, *et al*. (2005) Progressive adipocyte hypertrophy in aquaporin-7-deficient mice: Adipocyte glycerol permeability as a novel regulator of fat accumulation. *J Biol Chem* 280:15493–15496.
38. Maeda N, *et al*. (2004) Adaptation to fasting by glycerol transport through aquaporin 7 in adipose tissue. *Proc Natl Acad Sci USA* 101:17801–17806.
39. Hakimi P, *et al*. (2007) Overexpression of the cytosolic form of phosphoenolpyruvate carboxykinase (GTP) in skeletal muscle repatterns energy metabolism in the mouse. *J Biol Chem* 282:32844–32855.
40. Yeh JI, Du S, Tortajada A, Paulo J, Zhang S (2005) Peptergents: Peptide detergents that improve stability and functionality of an integral membrane protein, glycerol-3-phosphate dehydrogenase. *Biochemistry* 44:16912–16919.
41. Otwinowski Z, Minor W (1997) Processing of x-ray diffraction data collected in oscillation mode. *Methods Enzymol* 276:307–327.
42. Pflugrath JW (1999) The finer things in x-ray diffraction data collection. *Acta Crystallogr D* 55:1718–1725
43. Terwilliger TC, Berendzen J (1999) Automated MAD, MIR structure solution. *Acta Crystallogr D* 55:849–861
44. Murshudov, GN, Vagin AA, Dodson EG (1997) Refinement of macromolecular structures by maximum likelihood method. *Acta Crystallogr D* 53:240–255.
45. Brunger AT, *et al*. (1998) Crystallography and NMR system: A new software system for macromolecular structure determination. *Acta Crystallogr D* 54:905–921.
46. Perrakis A, Sixma TK, Wilson KS, Lamzin VS (1997) wARP: Improvement and extension of crystallographic phases by weighted averaging of multiple refined dummy atomic models. *Acta Crystallogr D* 53:448–455.